HHS Public Access

Author manuscript

Neuroimage. Author manuscript; available in PMC 2023 February 23.

Published in final edited form as:

Neuroimage. 2021 May 01; 231: 117818. doi:10.1016/j.neuroimage.2021.117818.

Infrared neural stimulation with 7T fMRI: A rapid in vivo method for mapping cortical connections of primate amygdala

Sunhang Shi[a,#], **Augix Guohua Xu**[a,#], **Yun-Yun Rui**[a], **Xiaotong Zhang**[a], **Lizabeth M. Romanski**[b], **Katalin M. Gothard**[c], **Anna Wang Roe**[a,*]

[a]Dept of Neurology of the Second Affiliated Hospital and Interdisciplinary Institute of Neuroscience and Technology, Zhejiang University School of Medicine, College of Biomedical Engineering & Instrument Science, Zhejiang University, Hangzhou, China

[b]Dept of Neuroscience, University of Rochester School of Medicine, Rochester, NY, United States

[c]Dept of Physiology, University of Arizona, Tucson AZ, United States

Abstract

We have previously shown that INS-fMRI is a rapid method for mapping mesoscale brain networks in the macaque monkey brain. Focal stimulation of single cortical sites led to the activation of connected cortical locations resulting in a global connectivity map. Here, we have extended this method for mapping brainwide networks following stimulation of single subcortical sites. As a testbed, we focused on the basal nucleus of the amygdala in the macaque monkey. We describe methods to target basal nucleus locations with submillimeter precision pulse train stimulation methods, and statistical tests for assessing non-random nature of activations. Using these methods, we report that stimulation of precisely targeted loci in the basal nucleus produced sparse and specific activations in the brain. Activations were observed in the insular and sensory association cortices as well as activations in the cingulate cortex, consistent with known anatomical connections. What is new here is that the activations were focal and, in some cases, exhibited shifting topography with millimeter shifts in stimulation site. The precision of the method enables networks mapped from different nearby sites in the basal nucleus to be

[*]Corresponding author. annawang@zju.edu.cn (A.W. Roe).
[#]Equal contributors

Credit author statement

Sunhang Shi : first author, conducted data collection and data analysis, made figures and wrote manuscript.
Augix Guohua Xu : first co-author, developed INS-fMRI method, developed grid and fiber pushing system, trained and supervised students in experiments and analysis, conducted data collection, wrote code for data analysis, made figures and wrote manuscript.
Yun-Yun Rui : helped with developing fiber pushing system, conducted some data acquisition and preliminary data analysis.
Xiaotong Zhang : made the RF coil, support on MR physics.
Lizabeth M. Romanski : provided anatomical knowledge and understanding of connectivity patterns, data interpretation, made figures and wrote manuscript.
Katalin M. Gothard : provided concepts of amygdala functional loops, provided understanding of amygdala structure, function and connectivity, co-supervised Yun-Yun Rui, made figures and wrote manuscript.
Anna Wang Roe : corresponding author, provided funding, supervision of method development, data analysis, made figures and wrote manuscript.

Declaration of Competing Interest

None.

Supplementary materials

Supplementary material associated with this article can be found, in the online version, at doi:10.1016/j.neuroimage.2021.117818.

distinguished. While further investigation is needed to improve the sensitivity of this method, our analyses do support the reproducibility and non-random nature of some of the activations. We suggest that INS-fMRI is a promising method for mapping large-scale cortical and subcortical networks at high spatial resolution.

Keywords

Infrared neural stimulation; Functional tract tracing; Macaque monkey; Basal nucleus of the amygdala; Connectome; High spatial resolution; Mesoscale

1. Introduction

Our understanding of functional networks in the brain depends strongly on the methodologies used to evaluate its connectivity. The different profiles of these methods offer distinct spatial and temporal resolutions, as well as local vs. global extents of circuit analysis. With the addition of new approaches to our toolbox, the view of the brain is modified, strengthened, and expanded. The introduction of MRI technology has led to a tsunami of studies on the circuit basis of behavior and cognition in humans. In resting state MRI studies, brain networks are inferred from temporal correlations between brain areas (typically with resolutions of 2–3 mm sized voxels). Diffusion based studies infer axonal trajectories by following water-based anisotropy. Based on these workhorse methods, human brain connectome projects [e.g. Human Connectome Project (USA), Brainnetome (China), Developing Human Connectome Project (Europe)] are now prime sources for many investigations of human brain function and disease. Despite these advances, methods with improved spatial resolution are needed to further define the functional specificities of brain networks.

Nonhuman primate (NHP) models of brain function can complement human studies and provide platforms for the development of new technologies. There are good reasons why NHPs have been longstanding models of human brain function. Not only do NHPs have behavioral repertoires similar to humans (including sensorimotor, cognitive, and social behaviors), NHP brains share more similarities with the human brain than rodents in terms of size, number of brain areas, and cortical organization. Advances in technologies for studying NHP brains with MRI methods now provide a direct link between human MRI studies and neuroanatomical, electrophysiological, and behavioral studies in NHPs.

One recent development in NHP MRI technology is a method for studying brain connections termed INS-fMRI (Xu et al., 2019). Infrared neural stimulation (INS), delivered via optic fibers, induces neuronal firing via optically induced heat transients. While the mechanism is still under study, it is believed that heat transients lead to changes in membrane capacitance and Na and K channel kinetics and subsequent neuronal response (Ganguly et al., 2019; Shapiro et al., 2012; Zhu et al., 2019). Applications of this method include stimulation of peripheral nerves (for muscle contraction, (Wells et al., 2005a)), the cochlea (to overcome deafness, Tan et al., 2018), and quail hearts (for pacemaking, Ford et al., 2018) (for review, see Chernov and Roe, 2014). When INS is used to stimulate focal (submillimeter) sites in the cerebral cortex, connected sites are activated and can be imaged using ultrahigh field

MRI; this results in a map of a brain-wide network connected to a single site. Feedforward and feedback connections can also be distinguished based on the laminar patterns of activation. Unlike optogenetics (e.g. (Gerits et al., 2012; Ohayon et al., 2013)), INS-fMRI can be readily applied to any location in the brain without prior viral transfection. Currently, it is the only method available for rapid, in vivo, high spatial resolution, brain-wide scale mapping of networks tied to single submillimeter points in the brain.

We previously developed INS-fMRI for mapping brain connections from single sites at the cortical surface, either with or without an intervening artificial dura (Cayce et al., 2014; Xu et al., 2019). Parameters for non-damaging stimulation were developed and intensity-dependent activations established (Cayce et al., 2014; Chernov and Roe, 2014). Based on a tissue penetration depth of about 300 μm (Wells et al., 2005a, 2005b), application of INS at the cortical surface was predicted to activate cells within the superficial layers of cortex as well as apical dendrites of deep layer pyramidal cells. The cortico-cortical and subcortical connections revealed were consistent with this prediction.

Here, we extend this capability by developing it for stimulation of deep brain sites. As a testbed, we focus on the amygdala of the macaque monkey, because it is considered one of the most interconnected subcortical hubs of the primate brain (Bickart et al., 2014; Tomasi and Volkow, 2011). Within the amygdala are two main groups of nuclei: (1) the basolateral group (including the lateral, basal, and accessory basal nuclei, that establish connections primarily with cortical areas), and (2) the centromedial group (including the central and medial nuclei, that establish connections primarily with subcortical structures) (Amaral et al., 1992). The basal nucleus of the amygdala is a region characterized by a diversity of neuronal responses and exhibits strong connections with major limbic as well as sensory association cortical areas. The circuits associated with the basal nucleus support its role in assigning behavioral significance of incoming stimuli (“what does it mean”) (Barbas, 2007; Pitkänen and Amaral, 1991). While the primary connectional targets of the basal nucleus, based on neuroanatomical tract tracing studies, are well known (for a review see (Shumann et al., 2016; Amaral et al., 1992)), relative differences in connectivity within this nucleus have been difficult to explore with traditional anatomical methods.

Here, we demonstrate that the INS-fMRI method can reveal known cortical connections of the basal nucleus of the amygdala and that stimulation of different sites within this nucleus activate distinct networks in the macaque monkey brain. We show that some of the known connections of the basal nucleus (Fig. 1) are reflected in our results, and furthermore, that these connections are more focal and specific than shown in previous anatomical studies utilizing large injections of tracers. These findings indicate that INS-fMRI is a promising novel method for mapping connections of deep brain structures at high spatial resolution.

2. Methods

2.1. Macaque monkeys

Two adult macaque monkeys were used (left and right amygdalae in Monkey M and right amygdala in Monkey Y). We have analyzed and present here 3 sessions and 7 stimulation sites from the left amygdala of monkey M and 2 sessions and 2 stimulation sites from

the right amygdala of monkey Y. In Monkey M Amygdala 1, 5 sessions were used to test different stimulation paradigms and intensities. Figs. 2–3 show data from 2 of these sessions. In Monkey M Amygdala 2, 4 sessions were conducted and 5 stimulation sites are presented from the basal nucleus of the amygdala. Figs. 4–8 show data from these sessions (4 stimulation sites along one penetration #27,#28,#29,#30 and 1 stimulation site from a second penetration #46 through the basolateral nucleus of the amygdala). In Monkey Y Amygdala 3, 9 sessions were conducted. We illustrate data from 2 sessions containing 2 basolateral stimulation sites in this monkey (Figs. 5 and 8). In Monkey M, a block design stimulation paradigm was used; in Monkey Y, an event-related stimulation paradigm was used (see below).

2.2. Animal preparation and surgery

Experiments were conducted in adult rhesus monkeys. All procedures were in accordance with NIH standards and with the approval of Zhejiang University Institutional Animal Care Committee. Minor surgery (drilling of burr hole) was conducted just prior to the scan in a surgical suite adjacent to the MR scanner. Monkeys were intubated, placed in a stereotaxic apparatus, and artificially ventilated. They were se-dated with ketamine hydrochloride (10 mg/kg)/atropine (0.03 mg/kg) and anesthetized with 1–2% isoflurane. After local infiltration of skin with lidocaine 1%, a small incision was made in the scalp and a small burr hole craniotomy was then performed at a stereotaxic location for targeting the basal nucleus of the amygdala. In Monkey M, a grid was implanted in one hemisphere to aid in the systematic targeting of multiple sites in different subnuclei of the amygdala. During the entire procedure the animal's body temperature was maintained at 37.5–38.5 °C with a water blanket. Vital signs (heart rate, SpO_2, end-tidal CO_2, and respiration rate) were continuously monitored. During the scan, monkeys were maintained with either (1) sufentanil (2 to 4 μg/kg per hour CRI (continuous rate infusion); induction, 3 μg/kg supplemented with 0.2–0.5% isoflurane or (2) propofol (2.5–5 mg/kg induction, 0.2–0.6 mg/kg/hr, supplemented with 0.2–0.5% isoflurane. Vital signs (heart rate, SpO_{2z}, end-tidal CO_2, respiration rate, temperature) were continuously monitored.

2.3. INS stimulation paradigm

We used two INS stimulation paradigms (see Cayce et al., 2014, Xu et al., 2019): (1) Event-related paradigm (see Fig. 3A) consisted of trains of optical pulses (1875 nm wavelength) with pulse widths of 250 μs delivered at 200 Hz for 0.5 s through a 200um diameter optic fiber. Thirty pulse trains were delivered during a period of 562 s. (2) In the block paradigm (see Fig. 5), each block consisted of a triplet of pulse ON trains (1x every 3 s) spanning a total of 9 s. The pulse ON blocks were repeated 20 times (once per 36 s) over a period of 720 s. Radiant exposures which were shown to be non-damaging (Chernov et al., 2014) ranged from 0.1–1.0 J/cm^2. As the fiber tip was in direct contact with tissue, for most of the sessions, we used conservative stimulation intensities of 0.1–0.3 J/cm^2. Block design intensities of 0.1 J/cm^2 were roughly equivalent to event-related design intensities of 0.3 J/cm^2. Each run (562 s for event-related, 720 s for block design) consisted of a single intensity. We used all trials in analyses and did not select trials.

2.4. Data acquisition procedure

Functional images of voxel size 1.5-mm-isotropic were acquired in a 7-Tesla MR scanner (Siemens, Erlangen, Germany) with a customized 6-channel receive coil (inner diameter 6–7 cm) with a single-loop transmit coil (inner diameter 18 cm) and a single-shot echo-planar imaging (EPI) sequence (TE 25 ms; TR 2000 ms; matrix size 86 × 72; flip angle 90°). This coil provided improved homogeneity of temporal signal-to-noise ratio (tSNR) over regular surface coils, resulting in images with similar tSNR values (mean tSNR of gray matter ~75). Functional images from opposite phase-encoding direction were also acquired for correction of image distortion (Andersson et al., 2003). In addition, Magnetization Prepared Rapid Acquisition Gradient-Echo (MPRAGE) sequence was used to get structural images of voxels size 0.3 and 0.5-mm isotropic.

2.5. Detection of significant responses

Structural and functional images in raw DICOM files from Siemens scanner were converted to NIfTI (Li et al., 2016) and AFNI format. Functional images were preprocessed with correction for slice timing, motion, image distortion and baseline shift. Significant responses were identified in a commonly used generalized linear model (GLM) approach, in which the timecourse of each voxel was regressed on the stimulus predictor (see Fig. 3). Stimulus predictor was the convolution between laser onsets and the standard hemodynamic response function. Regression coefficients were subjected to T-tests. Voxels with significant T-test p-values ($p < 0.0001$) were highlighted on top of the structural images. For some sessions, comparisons were made between the analyses at different thresholds ($p < 0.005$, $p < 0.001$,) and comparisons with and without the cluster size criteria (at least 5 neighboring voxels touching corners). Individual voxel timecourses were extracted from EPI data with AFNI (Cox, 2012) 3dmaskdump. Time-courses were then averaged over 20 or 30 repetitions and plotted. Each baseline was estimated with the mean MR signal over full timecourse. The analyses were done with software AFNI (Cox, 2012), Nipype (Gorgolewski et al., 2011), Bash, R and Python.

2.6. Half-data analysis

To test reproducibility, the full timecourses were divided into odd and even trials. This resulted in 2 halves of the data subjected separately to GLM tests. This also resulted in 2 sets of activation maps compared side by side (Fig. 6). The significant voxels (p-value < 0.0001) common to the 2 halves of the data were considered as reproducible.

2.7. Permutation test

We noted that not all activations survived the stringent cutoffs from standard GLM analysis. We believe that this may be due to the small number of trials collected and indicate that more trials are needed in future studies. To further examine the likelihood that these voxel patterns are due to random chance, we developed a permutation test which is a bootstrapping method for generating a distribution of chance levels. Our monkey fMRI data contains about 200,000 voxels. Therefore, the connection detection involves the simultaneous tests of hundreds of thousands of hypotheses. To correct for false positives (Type-1 errors), multiple testing correction has been performed. We do so with both Benjamini-Hochberg correction,

and the randomization-based permutation tests. In the permutation tests, we take the original timecourse of each voxel, and randomly shuffle the timepoint labels to create 10,000 new timecourses for each voxel. We then performed the same response detection analysis (fMRI GLM analysis) on these new timecourses. In this way, we get 10,000 new p-values from the randomized data. Lastly, we calculate the fraction of these p-values that are more or equally significant than the p-value from the real data. This fraction is the *permutation adjusted p-value (perm-p)* for the real data.

2.8. Image alignment

All structural and functional images were co-registered to the digital version of rhesus monkey atlas (Reveley et al., 2017; Saleem and Logothetis, 2012) with AFNI programs 3dAllineate and 3dNwarpApply. With these atlases, annotations of brain regions were then assigned to all imaged voxels. Stimulation sites were determined in structural images on which the tip of the optic fiber was dark and distinct from tissues (see Fig. 2C–F).

3. Results

For this study, we stimulated the left and right amygdala of monkey M and right amygdala of monkey Y. As a testbed for using the INS-fMRI method for stimulation in deep brain areas, we focused on the basal nucleus. This nucleus is the origin of robust projections to components of the limbic system, including sensory association areas such as the insula and the cingulate cortices (e.g. Amaral et al., 1992; Jezzini et al., 2015; Morecraft et al., 2007; Morecraft and van Hoesen, 1992).

To help establish and test the capabilities of this method, we developed methods to accurately target stimulation, tested intensity dependence of stimulation, and evaluated methods for quantifying activations in response to different stimulation paradigms. To test whether this method would reliably reveal activation of brain networks, we examined whether stimulation in the basal nucleus of the amygdala would: (1) activate insula and/or cingulate cortex, (2) would reveal focal or broad connections, and (3) would be useful for studying potential topography of networks associated with basal nucleus. Briefly, we find reliable activation in the insula and sensory association areas near the insula and weak activation in the cingulate.

3.1. Accurate targeting of the optical fiber and INS stimulation

The location of the fiber tip in the amygdala was assessed based on a high-resolution structural scan used to segment the amygdala into its component nuclei. The nuclear boundaries outlined in the structural images were then superimposed on the functional images. An example of how the stimulation site was anatomically localized is shown in Fig. 2. Using the stereotaxic coordinates calculated based on the initial structural scan (Fig. 2A, B), we precisely targeted a preselected site in the amygdala. An example of how the stimulation site was anatomically localized is shown in Fig. 2C–F. Based on stereotaxic coordinates (Saleem and Logothetis, 2012), we lowered a single 200um optic fiber into the brain to target the dorsal region of the basal nucleus of the amygdala. The fiber optic and its tip location was tracked by high resolution anatomical MPRAGE scans. In the coronal

plane, the presence of a vertical line of signal dropout (due to susceptibility artifact of the fiber glass) clearly identified the fiber location in the antero-posterior and medio-lateral axes (Fig. 2C). In the dorso-ventral axis, high resolution anatomical slices were obtained at 0.3 mm resolution. The tip location was determined by observing sequential horizontal slices. The fiber location (red circles) appears as a dot of signal dropout (Figs. 2 D and 2E) and disappears in Fig. 2F; we therefore inferred the fiber tip location to be at the horizontal level of Fig. 2E. This determination has an error of not more than 0.3 mm, sufficiently precise for amygdala subnuclear localization.

3.2. Intensity-dependent response at the laser tip

As shown in Fig. 2, INS stimulation of an optic fiber placed in the dorsal region of the basal nucleus of the amygdala resulted in activation at the fiber tip (red voxels). At a stimulation intensity of 0.3 J/cm^2, the stimulation site is quite clear and focal ($p < 0.001$). By varying the stimulation intensity from 0.1 – 0.7 J/cm^2, a clear intensity-dependence was observed, as shown in the BOLD signal response (Fig. 2H: left, colored lines; right, plotted against radiant exposure). This intensity-dependent BOLD relationship suggests that increasing INS intensity leads to increased neuronal response.

3.3. INS stimulation paradigm reveals activations at connected sites

Previously we developed INS stimulation paradigms that employed trains of optical pulses with pulse widths of 250 μs delivered at 200 Hz for 0.5 s through a 200 μm diameter optic fiber (Cayce et al., 2014; Xu et al., 2019). As determined by water absorption characteristics, INS stimulation was spatially confined to a small volume of brain tissue, roughly a few hundred microns in diameter (Cayce et al., 2014; Wells et al., 2005a). Radiant exposures from 0.1–1.0 J/cm^2 were shown to be non-damaging (Chernov and Roe, 2014). Here given that the tip is surrounded by tissue without any intervening artificial dura, we conservatively reduced our stimulation intensities to 0.1–0.7 J/cm^2. In practice, as illustrated below, we find that radiant energies of 0.1–0.3 J/cm^2 in the amygdala were sufficient to achieve activation at connected sites.

We experimented with two types of stimulation paradigms in the amygdala: event-related and block design. The event related stimulation method is shown in Fig. 3. Thirty pulse trains (Fig. 3A, below, red vertical line: one pulse train) were delivered during a period of 562 s. Stimulations were delivered at random intervals (between 10 and 28 s) to reduce false positives (e.g. from simple oscillations). The duration of each pulse train was 0.5 second and consisted of 100 pulses of 250 μs (expanded in Fig. 3A, above). Voxel responses were tracked over time (Fig. 3B). As shown in Fig. 3C, each pulse train led to a robust and reliable BOLD response at the laser tip and produced a high correlation value ($r = 0.85$). Time-courses were then averaged over 30 repetitions and plotted (Fig. 3D). In the block design method (shown in Fig. 5), each block consisted of a triplet of pulse ON trains (1x every 3 s) spanning a total of 9 s. The pulse ON blocks were repeated 20 times (once per 36 s) over a period of 720 s; thus, effectively the interstimulus period was 29.5 s. We found that, while event-related stimulation is most similar to our optical imaging methods, it achieves comparatively weak activation at connected sites (Fig 3E, $r = 0.31$, averaged timecourse shown at right). Block design is more robust and reliable (see Fig. 5). Note

that, to permit visualization of focal activations, cluster size criteria were generally not used (see Fig. 8). Both designs produced very focal stimulation sites (typically single voxel). This is consistent with the delivery of a spatially and temporally confined heat bolus to the tissue (thermal confinement regime of energy transfer to water, Wells et al. 2005) and also consistent cortical stimulation studies (Xu et al., 2019); optical imaging studies have shown that stimulation at these intensities remain focal and submillimeter in size (Cayce et al., 2011, 2014). We did not find any evidence of 'spreading' of activation'.

At each stimulation site, we conducted multiple runs of INS stimulation. Each run consisted of a single intensity, delivered with either event-related or block design. Typically, data from 3–4 intensities would be acquired at each site. After completion of data collection from a site, the fiber would be advanced further downward, another high spatial resolution anatomical run was acquired for tip localization, and another series of acquisitions was obtained. Typically, 3–4 sites would be studied in a single penetration. Upon completion of the session, the fiber would be removed and the animal recovered.

3.4. Stimulation of punctate sites in the amygdala resulted in discrete remote activations

We show full slices resulting from stimulation in a single site in the basolateral nucleus of the amygdala in Monkey M. Fig. 4 shows all coronal slices of Site 28 stimulation (0.1 J/cm^2, $p < 0.0001$, FDR 5.5%); this site contributed to Fig. 5E–H (slices outlined in yellow), and Fig. 7D (slices outlined in blue). These slices illustrate the specificity of connected sites and that activated sites are quite focal. This sparsity is typical of what we observe in all of our stimulation sites. We next sought to evaluate whether these activations could be compatible with known anatomical connections or whether they are simply noise.

3.5. Activations are consistent with known anatomical connections: insula & lateral sulcus

An example result of INS stimulation is illustrated in Fig. 5. In this case, the fiber tip was estimated to be localized to the intermediate region, between the magnocellular and parvocellular regions of the basal nucleus (Fig. 5A and B). The stimulation of this site resulted in the activation of a distinct cluster of voxels (E-H: $p < 0.0001$, FDR 5.5%) in the insula (representative schematics of insula shown in 5C and D), as well as small patches of cortex in the surrounding lateral sulcal regions that extended anterior-posteriorly from +9.5 mm to +17 mm. Notably, these clusters were focal and sparse, leading to an impression of high specificity.

Figs. 5 E–H show the pattern of activation in four different coronal sections along the anterior-posterior axis of the brain. The activated voxels included the retroinsular region and the granular and dysgranular insula (Id) (5E through H), auditory areas CM, RM and R, as well as patches of the secondary somatosensory cortex SII. The anteroposterior extent of insular activation parallels the previously described 'insular stripes' within the dysgranular insula (Evrard, 2019). Moreover, this stripe-like activation falls primarily in the ventral portion, a region which corresponds to dysgranular insula, consistent with labeling from anatomical tracer injections in basal and basal accessory nuclei (Amaral and Price, 1984; Jezzini et al., 2015). The strong insula activation is surrounded by light

activation in secondary somatosensory cortex and medial belt auditory cortical activation. Single voxel activations were seen in SII and perhaps area 7 in Fig. 5E–G. In auditory cortex the activation included both rostral (R, RM) and caudal (CM) auditory core and belt subdivisions of the auditory cortex. This pattern of activation corresponds to some of the connectivity patterns previously shown in tract tracing studies (summarized by Amaral et al., 1992 and confirmed with additional details by Barbas and de Olmos, 1990; Ghashghaei and Barbas, 2002; Jezzini et al., 2015; Yukie, 2002), though studies have focused on cortico-cortical connections in auditory belt cortex rather than subcortical regions (Hackett et al., 2014; Smiley et al., 2007). The difficulty of stimulating exactly the same subnuclear site of the amygdala and the considerable inter-individual variations in connectivity may explain the observed differences.

We then examined the timecourses of the BOLD activations at these presumed connected sites. Significant voxels were selected at a level of $p < 0.0001$. The average time course of the fMRI signal in these voxels (shown in Figs 5I–L) show increased fMRI signals at the expected latency after the stimulus triplet (vertical red lines) and with a magnitude consistent with the BOLD response.

We show that an event related stimulation paradigm could achieve similar results (the right amygdala in monkey Y, Fig. 5M–P). This also resulted in ipsilateral activation sites in the insula and in somatosensory cortex but no activation in auditory areas. However, the significance of responses in this case was lower ($p < 0.001$, FDR 7.7%), illustrating the weaker effect of this stimulation paradigm.

3.6. Reliability of activation patterns

We carried out additional tests to examine the possibility that the observed activations were due to noise. Indeed, the punctate and relatively sparse distribution of activated voxels raised the possibility that the active voxels are due to random fluctuations. If this were the case, it would predict a high degree of variability in activation from one stimulation event to the next. That is, the small number of voxels activated by each stimulation would be in different locations generating non-overlapping maps across stimulations. If, however, the pattern of activation is not random, the activation pattern would tend to show significant overlap across trials even if on some trials the voxels in question fail to cross threshold. Indeed, if the laser tip activates only a few voxels in the amygdala, we expect the remote activation to vary in intensity but not in location.

To test the reliability of the observed activation patterns, we took the data from one run at stimulation site #30 (20 stimulations) and split them into two groups of 10; one block contained the odd trials and the other 10 the even trials. We then compared the activations between these two blocks of trials. Fig. 6A shows the activation maps derived from the odd trials and Fig. 6B from the even trials (with a threshold of $p < 0.0001$, FDR 6.7%). We observed that overall, these maps were highly similar. Similar to what is seen in Fig. 5, common sites were located in the insula, SII, and auditory cortex. It appears that the activations within the lateral sulcus are largely reproducible. We conclude that if the same cluster of voxels are activated on a different half set of trials within the same run, then it is likely to reflect a reliable connection.

We also used a statistical argument to evaluate the possibility that the observed activation pattern can be explained by random fluctuations. We shuffled the location of the significant voxels across all possible voxels. In a single scan, there are 36,030 voxels in a single EPI image, and 222,912 voxels in the entire monkey brain. For example, we took the 70 significant voxels (p-value 0.0001) from stimulation site #30 (Fig. 6) and noted that 50 voxels were located in the lateral sulcus. We than performed both Fisher's exact test and a simulation test to estimate the probability for a such clustering in the lateral sulcus. In the Fisher's exact test, we found that voxel significance and location in the lateral sulcus are independent events (p-value < 2.2e-16, odds ratio 764), i.e., there is an enrichment of significant voxels in the lateral sulcus (defined here as a combination of brain regions CM, RM, R, SII, Ig, Id, Ri, 7op, A1, AL), resulting in 771 voxels within the lateral sulcus. For the simulation test, we randomly sampled 70 significant voxels over the whole brain, and then counted the number of significant voxels located in lateral sulcus. We repeated this for 100,000 simulations (See Supplementary information). We found that in most of the simulations (79%), there were no significant voxels located in the lateral sulcus. In some simulations (19%), we found only 1 significant voxel in the lateral sulcus. None of the random samplings resulted in 50 voxels in lateral sulcus. We therefore conclude that the probability for our enrichment of 71% (50 out of 70) significant voxels in lateral sulcus is virtually 0 by chance.

3.7. Topography of connectivity: nearby sites in the amygdala activate nearby voxels

In sensory (and motor) systems there are well-established topographic relationships between the thalamic and cortical maps. For example, a 'point-to-point' mapping has been described in the visual system for the connectivity between the lateral geniculate nucleus of the thalamus and the primary visual cortex. However, little is known about the topography of connectivity between single nuclei in the amygdala and cortical target areas. Here, we examined whether focal stimulation of sequential points in the amygdala might reveal shifting activations in the cortex.

We stimulated three sites within the basal nucleus of the amygdala. Two of the stimulation sites were co-linear in the vertical axis (Fig. 7A–B, sites D and E indicated by upper and lower red dots). A third stimulation site (site F on Fig. 7A) was slightly more medial from the other two sites. All three sites were located in the basal nucleus of the amygdala spanning the intermediate and parvocellular portions of the basal nucleus (Fig. 7A) most likely including portions of the intermediate and parvocellular subdivisions. Activations in the lateral sulcus from each of the sites are shown in Fig 7D, E, F with corresponding atlas sections at AP +17, 14, 11 and 8 depicted in 7C. We observed that these stimulations all resulted in varying degrees of activation in neighboring sites including the insula (Id, Ig, Pi, Ri), somatosensory (SII), and auditory cortical areas (AL, R, RM, CM) (see Fig 7C). As shown in Fig. 7D, stimulation at the dorsal site produced activations in auditory (AL, R) and insula (Id) at AP+17; auditory (RM), insula (Id, Ig), and SII at AP+14; insula (Id,Ig) and somatosensory (SII, 1–2) at AP +11; and a single voxel in CM at AP +8. The next site of stimulation was about 2 mm ventral to that and was most likely in the parvocellular subdivision of the basal nucleus (Fig. 7A). As shown in Fig. 7E, the stimulation of this site produced more robust and quasi-overlapping activation with the dorsal site. Specifically, at

AP+17 separate clusters of activations are present in AL, R and RM while at AP+14 intense activation of RM, Id and SII is present. This is even more pronounced at AP+11. Caudally at AP+8, two small foci of activation occur in parietal area 7op and 7b. The third stimulation site in Fig. 7F, located slightly medial to that in 7E, resulted in a much weaker pattern of activation in all areas. Note the very focal (1–2 voxel) activations rostrally in the insula and the claustrum at AP+17. At AP +11, there were single voxel activations in insula and somatosensory cortex (SII), while at AP+8 focal activations were found in insula (Id, Ig), caudal insular region Ri, and 7op.

In sum, the most dorsal site, D, in the intermediate basal nucleus, evoked robust activation in insula (Id, Ig, Ri), with some focal activations in auditory (RM) and somatosensory cortex (SII). From the medial site, E, similar but stronger activations appeared in the auditory, insula and somatosensory cortices. In contrast, the ventral most site, F, notably lacked much auditory or somatosensory activation, and predominantly led to focal activations in insula, as well as in claustrum. These activation patterns point to different profiles of activation in the dorsal/middle, and ventral regions of the basal nucleus, echoing an even more discrete topography than can be seen with most studies of anatomical tract tracing (Price, 1999).

3.8. Activations of cingulate cortex

We also examined activation in the cingulate cortex (Fig. 8). Three examples are shown from 2 hemispheres in two monkeys and they illustrate the results of somewhat different stimulation paradigms and different analysis methods. In both monkeys the stimulation sites were located in the basolateral nucleus of the amygdala (shown in Fig. 8A–C). In Monkey M (Fig. 8A, 8D, stimulation site #46; Fig. 8B, 8E, stimulation site #27), data were collected with block design; in Monkey Y (Fig. 8C, 8F), data were collected with event-related design. We also show two methods of evaluating the data: standard GLM analysis for voxel significance and a permutation adjusted p value analysis for assessment of deviation from chance levels.

As shown in Fig. 8D (Monkey M Site #46, $p < 0.0001$, FDR 11.6%), several patches (yellow arrowheads) of activation are observed over the antero-posterior expanse of the cingulate cortex (areas 23 and 24). In addition, two other activations appeared in retrosplenial (area 30) and medial parietal (area 7) locations. In Fig. 8E (Monkey M Site #27, permutation adjusted $p < 0.002$, see Methods), a pattern of patches along the cingulate in areas 23 and 24 was also observed; in addition, 2 patches were observed in medial prefrontal 25 and 32. In Fig. 8F (Monkey Y, $p < 0.001$), similar focal activations in the cingulate were also observed, although significance was weaker due to the event-related paradigm. In all 3 cases, activations were observed in the cingulate, consistent with expectations from anatomical tracer studies (cf. Morecraft et al., 2007, Loh et al. 2018).

In contrast to anatomical studies, connectivity patterns consisted of a high degree of focal patches; these patches are not due to ghosting (Supp Fig. 1). The patches in the three cases are in slightly different locations along the cingulate, likely due to the different locations of stimulation sites in the amygdala. We suggest these may relate to the known face, arm, and leg motor topography in each of areas 23 and 24 previously shown in monkey (Morecraft et al., 2007) and human cingulate (Loh et al. 2018).

We also examined alternative ways to assess randomness. When the permutation test (see Methods) was applied to the data from Monkey M site #27, we found that the several patches in cingulate cortex survived the test to a level of perm-$p < 0.002$ (Fig. 8E); these included 3 cingulate patches and 2 medial prefrontal patches. The randomized timecourses do not show better correlation with the stimulus paradigm for these patches. Moreover, no other voxels appear to be significant. Thus, this suggests that at least some of the cingulate connectivity and medial prefrontal connectivity is non-random. However, further studies are required to further verify these findings.

In sum, stimulation of a single focal submillimeter site in the basal nucleus of the amygdala revealed a network of focal nodes in different locations in the anterior and posterior cingulate cortex (Morecraft et al., 2007) and the medial prefrontal cortex (Carmichael and Price, 1995; Price, 1999; Sharma et al., 2020), sites that are consistent with the known anatomical connectivity of the basal nucleus. Note that we do not see statistically significant voxels in orbitofrontal cortex, entorhinal cortex, perirhinal cortex, the anterior temporal pole. This may be because the several sites studied here did not connect to these areas; alternatively, this may be due, in part, to the loss in signal-to-noise at the base of the brain due to proximity to the sinuses. Stimulation of single sites outside the amygdala (e.g. a site in the putamen, Supp Fig. 2) revealed connectivity quite distinct from that of the basal nucleus. Importantly, in a manner that is not always evident from anatomical studies these inferred connections were highly focal and patchy. Together these results suggest that INS induced activations were not random or non-specific and the INS-fMRI method can reveal, and potentially discriminate between highly specific and focal network maps.

4. Discussion

Development of focal deep brain stimulation method.

We have previously shown that laser-fMRI stimulation (neural infrared laser stimulation applied focally to an area of the cortical surface smaller than 0.5 mm in a highfield MRI) activates mesoscale networks. These networks are consistent with anatomical networks connected to the stimulated site (Xu et al., 2019). Here, we investigated whether a similar approach can reveal broader cortical networks associated with single subcortical stimulation site. We chose to stimulate the basal nucleus of the amygdala because this nucleus is a hub of connectivity where multiple cortical-amygdala processing loops intersect (Bickart et al., 2014; Gothard 2020). As such, the basal nucleus is the origin of numerous projections that target limbic and sensory cortical areas. These projections are likely to signal the affective and social significance of sensory stimuli computed by the basolateral nuclei of the amygdala. To target this small region of the brain (roughly $5 \times 5 \times 5$ mm in size), we developed new methodologies to reliably activate submillimeter locations online within the MRI (to within 0.3 mm resolution). We also developed methods to achieve reliable, intensity-dependent stimulation, and showed that both event-related and block design paradigms are capable of revealing consistent BOLD activations in target sites. Some sites exhibited strong connectivity, while others require greater number of trials to achieve a similar level of activation.

Multiple lines of evidence suggest that these connections are real and non-random.

Despite the relative sparseness and, in some cases, weakness, of these activations, we find their specificity of connectivity to be rather compelling. Several aspects of these activation sites indicate they are not random or non-specific activations. (1) Activation patterns matched known anatomical targets of the basal amygdala, especially efferent projections of the basal nucleus. (2) From a single stimulation site in the basal nucleus, activations over 7 mm of slices revealed stable activation profiles in the insula, somatosensory, and auditory cortices (Fig 5). (3) Activations exhibited focal, patchy profiles (Figs 4–8), reminiscent of cortical connectivity patterns and known functional organizations. (4) Spatially shifted stimulation sites within the basal nucleus gave rise to spatially shifted activation patterns that were partially overlapping and functionally consistent (Fig. 7). (5) Lateral sulcus and cingulate targets were demonstrated following stimulation of several sites and in two animals (Fig. 3-8). (6) Single voxel activations appeared to be highly specific, such as that in the claustrum and in each of auditory areas AL, R, and RM (Fig. 7), or in the medial prefrontal cortex and in the retrosplenial cortex (Fig. 8). (7) Some activations, such as that in the insula, survived half and half analysis (Fig. 6). (8) Stimulation of non-amygdala sites failed to elicit the activation of the targets activated by amygdala stimulation (Supp. Fig. 2). (9) We further tested for the possibility that activations were due to random noise. We used voxel shuffling to show that the likelihood of achieving the observed voxel pattern was extremely low and our calculations of the permutation adjusted p value (from bootstrapping the voxel timecourses) supported the non-random nature of weak responses (Fig. 8). Thus, we believe that, on the whole, these activations were not spurious and reflect true connectivity.

INS-fMRI may become a new addition to the existing toolkit.

Stimulation in conjunction with fMRI has been previously used for mapping of cortical networks. Tolias et al. (2005) first demonstrated that electrical stimulation in monkey V1 in the fMRI (es-fMRI) could reveal activation at connected sites in V2/V3 and MT. In a study that directly compared electrical stimulation with resting state connectivity, Matsui et al. (2011) reported that electrically evoked intrahemispheric connections reflected anatomical connectivity, whereas interhemispheric connectivity was likely due to synchrony arising from complex network interactions. In humans, Oya et al. (2017) mapped effective connectivity using intracranial electrical stimulation and fMRI. Optogenetics has also contributed cell-type specific approaches to mapping circuits and simultaneously examining modulatory effects of such stimulation in the MRI (Leong et al., Gerits et al., 2012, Ohayon et al., 2013). These have been the pioneers of functional circuit mapping from single node stimulation in the brain.

Adding INS-fMRI to these methods has several advantages. The primary advantage of this method is the focality of the energy delivery. Compared to other stimulation methods used in conjunction with MRI, the INS stimulus is relatively small and focal. The stimulus is a brief train of transient light-induced heat pulses (250us/pulse, 100 pulses delivered over 0.5 s). While the mechanism is still under study, it has been shown that delivery of near infrared light to tissue at wavelengths corresponding to the peaks of water absorption leads to efficient energy transfer and drives action potentials effectively (Cayce et al., 2014;

Wells et al., 2005b). As shown with optical imaging and electrophysiological methods, the effect of INS stimulation delivered through a 200um fiber optic is confined to single ocular dominance columns (~0.4 mm wide), resulting in highly specific activation of eye-matched local cortical networks (Cayce et al., 2014); this result parallels similar studies conducted with optogenetics (Chernov et al., 2018). Thus, in deep tissue, we estimate that the effective volume of tissue activated through a 200um fiber optic is also submillimeter in size. Moreover, given that we have conservatively stayed in the 0.1–0.3 J/cm^2 intensity range, it is likely that the effective volume is within ~0.5 mm. In sum, unlike electrical stimulation, INS-fMRI does not suffer from current spread or from significant MRI signal dropout at the electrode tip. It is also simpler to use than optogenetics as no viral transfection is required to achieve sensitivity to optical stimulation, making all sites in the brain potential targets for stimulation. However, its shortcoming is the lack of cell type specificity. We suggest that INS-fMRI guided optogenetic injections and electrical recording may be part of a future systems neuroscience strategies.

The BOLD signals at connected sites are not due to heat effects.

In the MRI, temperature changes are accompanied by resonance frequency shifts. This means that at the fiber optic stimulation site at least part of the ‘activation signal’ is due to some non-neural component related to temperature change. However, at connected sites, the signal is not due thermal effects and is most likely due to BOLD derived from post-synaptic activation (Xu et al., 2019). We have confirmed this with both experimental and modeling methods (Zhang et al., 2019).

INS revealed discrete and punctate connectivity from the basal nucleus.

We show that stimulation of the basal nucleus activates individual voxels or small clusters of voxels in the cingulate, insula, auditory, somatosensory, and association areas of the temporal cortex, consistent with the known anatomical connections reported by tract tracing studies (Amaral et al., 1992; Buckwalter et al., 2008; Evrard, 2019; Freese and Amaral, 2005; Jezzini et al., 2015; Morecraft et al., 2007; Morecraft and van Hoesen, 1992; Smiley et al., 2007; Stefanacci and Amaral, 2002; Yukie, 2002). Distinct from traditional anatomical studies, the activations were sparse and more focal than revealed by traditional anatomical tracing studies. Indeed, one of the primary and important points of this study is the idea that amygdala connectivity is highly specific at a local millimeter scale. That is, in contrast to anatomical tracers which label a relatively large cluster of projection neurons at the injection site, focal INS stimulation activates a small cluster of neurons which project in a highly specific way to discrete sites in the cortex and other targets. Similar, precise patterns of connectivity have been demonstrated with small tracer injections in many brain regions in multiple species and it is encouraging to see it replicated with this method with even more focal precision. Therefore, each focal stimulation site produces a subset of activation targets previously evoked by larger stimulation sites, but may not activate all the sites expected due to a specific spatial placement of the laser. This potentially offers important mm-scale topographic and functional specificity to our understanding of amygdala connectivity.

The focal nature of these connections is reminiscent of previously described anatomical patchy cortical connections and is in line with the column-specific connectivity patterns

found in the visual system. A potentially important application of this method is mapping the topography of connectivity in the brain. Our data show that details of the connectivity pattern change from one locus to another within the basal nucleus, providing a novel instrument to explore shifting patterns of connectivity in vivo (Fig. 7). We also suggest that the patchy pattern observed along the cingulate (Fig. 8) reflects the known face, arm, and leg motor topography in each of areas 23 and 24 previously shown in monkey (Morecraft et al., 2007) and human (Loh et al. 2018) cingulate. This technique may therefore overcome the challenges of achieving the placement of multiple, closely spaced, non-contiguous, small tracer injections in traditional tract tracing studies. In sum, results from basal nucleus of the amygdala open possibilities for studying point-to-point brain connections from deep structures in vivo.

Potential sources of weak BOLD correlations.

Due to the highly focal nature of INS stimulation, the methodology for routinely achieving strong, reliable signal remains to be improved. Fluctuation in anesthetic plane and the associated baseline variability may be one possible cause of weak connectivity. Another factor may be the presence of ongoing low frequency oscillations in the brain. In event-related stimulation paradigm, we randomized our stimulation to avoid stimulating at commonly encountered frequencies of slow oscillations. However, comparison of randomized and non-randomized event-related runs did not reveal any statistically significant differences (not shown). It may be that in many cases the activation is weak but the connection is not. For example, the small number of stimulated neurons may give rise to multiple axon collaterals which spread across the target in a patchy manner, resulting in weak activations. In contrast, targets like the insula may be loci of strong axonal convergence, resulting in a stronger activation. Other differences in activation profiles, such as feedforward vs feedback type connections, may also result in quantitative response magnitude differences. Importantly, there is always the issue of signal dropout near sinuses at the base of the skull (e.g. orbitofrontal cortex or entorhinal and perirhinal cortices) which may also contribute to a lack of strong activation. Finally, inter-individual variation in the anatomy of the amygdala or in amygdala-cortical connectivity may explain why we did not replicate every detail of the activation pattern between monkey M and Y.

Limitations of this method.

Despite the exciting capabilities of this method, there remain several limitations. (1) It is unclear whether the connectivity inferred from the activation pattern correspond to monosynaptic or polysynapic connections. Previously, we had shown that many voxels were consistent with monosynaptic connectivity and some voxels consistent with disynaptic connectivity (e.g. V1 to contralateral thalamus). We also showed that trisynaptic connectivity is unlikely, due to declining signal strength at each subsequent synapse (Xu et al., 2019). (2) Based on experiments thus far, it is unclear whether activations reflect afferent or efferent basal amygdala. However, additional high spatial resolution laminar imaging may provide the needed information to distinguish feedforward vs. feedback connectivity (Xu et al., 2019). (3) Whether this method is effective at revealing diffuse connections also remains unknown. It is possible that weak or diffuse connections may not achieve statistical significance and would fail to be revealed. These limitations also point toward ways to

improving this method. A more systematic mapping of connectivity with larger numbers of trials where each stimulation site is activated multiple times to test and re-test the activation patterns across time would undoubtedly bring to light the power and promise of this method.

Supplementary Material

Refer to Web version on PubMed Central for supplementary material.

Acknowledgments

This work was supported by: National Key R&D Program of China 2018YFA0701400 (to A.W.R.), Chinese NSF Instrumentation Grant No. 31627802 (A.W.R.), Key Research and Development Program of Zhejiang Province 2020C03004 (to A.W.R.), Fundamental Research Funds for the Central Universities 2019XZZX003-20 (to A.W.R.), China-US grant (NSFC 81961128029 to A.W.R., 1R01MH121706 to K.M.G.), National Natural Science Foundation of China (81701774, 61771423 to Xiaotong Zhang), Zhejiang Lab (2018EB0ZX01, to Xiaotong Zhang), and Key-Area Research and Development Program of Guangdong Province (2018B030333001, to Xiaotong Zhang). We acknowledge the following for their roles in experimental data collection: Gang Chen, Hsin-yi Lai, Xiao Du, Meizhen Qian, Shuxian Qu, Zhiyan Quan, Toru Takahata, Jianbao Wang, Pingyi Wang, Wang Xi, Bin Xu, Songping Yao, Hong Yin, Jichao Yu, Xiongjie Yu, Yuying Zhai, Xiaotong Zhang, Ying Zhang, Dengfeng Zhou, Liang Zhu.

Data and code availability statement

We will make data available to those who request it. A formal data sharing agreement will be established.

References

Amaral D, Price J, Pitkanen A, Carmichael ST, 1992. Anatomical organization of the primate amygdaloid complex, in the Amygdala: neurobiological aspects of emotion, memory, and mental dysfunction. Ed. J Aggleton 1–66.

Amaral DG, Price JL, 1984. Amygdalo-cortical projections in the monkey (Macaca fascicularis). J. Comp. Neurol 230, 465–496. doi: 10.1002/cne.902300402. [PubMed: 6520247]

Andersson JLR, Skare S, Ashburner J, 2003. How to correct susceptibility distortions in spin-echo echo-planar images: application to diffusion tensor imaging. Neuroimage 20, 870–888. doi: 10.1016/S1053-8119(03)00336-7. [PubMed: 14568458]

Barbas H, 2007. Flow of information for emotions through temporal and orbitofrontal pathways. J. Anat 237–249. doi: 10.1111/j.1469-7580.2007.00777.x. [PubMed: 17635630]

Barbas H, de Olmos J, 1990. Projections from the amygdala to basoventral and mediodorsal prefrontal regions in the rhesus monkey. J. Comp. Neurol 300, 549–571. doi: 10.1002/cne.903000409. [PubMed: 2273093]

Bickart KC, Dickerson BC, Barrett LF, 2014. The Amygdala as a Hub in Brain Networks That Support Social life, Neuropsychologia. Elsevier Ltd doi: 10.1016/j.neuropsychologia.2014.08.013.

Buckwalter JA, Schumann CM, Van Hoesen GW, 2008. Evidence for direct projections from the basal nucleus of the amygdala to retrosplenial cortex in the Macaque monkey. Exp. Brain Res 186, 47–57. doi: 10.1007/s00221-007-1203-x. [PubMed: 18049816]

Carmichael ST, Price JL, 1995. Limbic connections of the orbital and medial prefrontal cortex in macaque monkeys. J. Comp. Neurol 363, 615–641. doi: 10.1002/cne.903630408. [PubMed: 8847421]

Cayce JM, Friedman RM, Chen G, Jansen ED, Mahadevan-Jansen A, Roe AW, 2014. Infrared neural stimulation of primary visual cortex in non-human primates. Neuroimage 84, 181–190. doi: 10.1016/j.neuroimage.2013.08.040. [PubMed: 23994125]

Cayce JM, Friedman RM, Jansen ED, Mahavaden-Jansen A, Roe AW, 2011. Pulsed infrared light alters neural activity in rat somatosensory cortex in vivo. Neuroimage 57, 155–166. doi: 10.1016/j.neuroimage.2011.03.084. [PubMed: 21513806]

Chernov M, Roe AW, 2014. Infrared neural stimulation: a new stimulation tool for central nervous system applications. Neurophotonics 1, 011011. doi: 10.1117/1.NPh.1.1.011011.

Chernov MM, Chen G, Roe AW, 2014. Histological assessment of thermal damage in the brain following infrared neural stimulation. Brain Stimulat 7, 476–482. doi: 10.1016/j.brs.2014.01.006.

Chernov MM, Friedman RM, Chen G, Stoner GR, Roe AW, 2018. Functionally specific optogenetic modulation in primate visual cortex. Proc. Natl. Acad. Sci. U. S. A 115, 10505–10510. doi: 10.1073/pnas.1802018115. [PubMed: 30257948]

Cox RW, 2012. AFNI: what a long strange trip it's been. Neuroimage 62, 743–747. doi: 10.1016/j.neuroimage.2011.08.056. [PubMed: 21889996]

Evrard HC, 2019. The organization of the primate insular cortex. Front. Neuroanat. Front. Media S.A doi: 10.3389/fnana.2019.00043.

Ford S, Watanabe M, Jenkins M, 2018. A review of optical pacing with infrared light. J. Neural Eng 15, 011001. doi: 10.1088/1741-2552/aa795f.

Freese JL, Amaral DG, 2005. The organization of projections from the amygdala to visual cortical areas TE and V1 in the macaque monkey. J. Comp. Neurol 486, 295–317. doi: 10.1002/cne.20520. [PubMed: 15846786]

Ganguly M, Ford JB, Zhuo J, McPheeters MT, Jenkins MW, Chiel HJ, Jansen ED, 2019. Voltage-gated potassium channels are critical for infrared inhibition of action potentials: an experimental study. Neurophotonics 6, 040501. doi: 10.1117/1.NPh.6.4.040501.

Gerits A, Farivar R, Rosen BR, Wald LL, Boyden ES, Vanduffel W, 2012. Optogenetically-induced behavioral and functional network changes in primates.Curr. Biol. CB 22, 1722–1726. doi: 10.1016/j.cub.2012.07.023. [PubMed: 22840516]

Ghashghaei HT, Barbas H, 2002. Pathways for emotion: interactions of prefrontal and anterior temporal pathways in the amygdala of the rhesus monkey. Neuroscience 115, 1261–1279. doi: 10.1016/S0306-4522(02)00446-3. [PubMed: 12453496]

Gorgolewski K, Burns CD, Madison C, Clark D, Halchenko YO, Waskom ML, Ghosh SS, 2011. Nipype: a flexible, lightweight and extensible neuroimaging data processing framework in python. Front. Neuroinformatics 5, 13. doi: 10.3389/fn-inf.2011.00013.

Hackett TA, de la Mothe LA, Camalier CR, Falchier A, Lakatos P, Kajikawa Y, Schroeder CE, 2014. Feedforward and feedback projections of caudal belt and parabelt areas of auditory cortex: refining the hierarchical model. Front. Neurosci 8. doi: 10.3389/fnins.2014.00072.

Jezzini A, Rozzi S, Borra E, Gallese V, Caruana F, Gerbella M, 2015. A shared neural network for emotional expression and perception: an anatomical study in the macaque monkey. Front. Behav. Neurosci 9. doi: 10.3389/fnbeh.2015.00243.

Li X, Morgan PS, Ashburner J, Smith J, Rorden C, 2016. The first step for neuroimaging data analysis: DICOM to NIfTI conversion. J. Neurosci. Methods 264, 47–56. doi: 10.1016/j.jneumeth.2016.03.001. [PubMed: 26945974]

Matsui T, Tamura K, Koyano KW, Takeuchi D, Adachi Y, Osada T, Miyashita Y, 2011. Direct comparison of spontaneous functional connectivity and effective connectivity measured by intracortical microstimulation: an fMRI study in macaque monkeys. Cereb. Cortex 21 (10), 2348–2356. [PubMed: 21368090]

Morecraft RJ, Mcneal DW, Stilwell-Morecraft KS, Gedney M, Ge J, Schroeder CM, Van Hoesen GW, 2007. Amygdala interconnections with the cingulate motor cortex in the rhesus monkey. J. Comp. Neurol 500, 134–165. doi: 10.1002/cne.21165. [PubMed: 17099887]

Morecraft RJ, van Hoesen GW, 1992. Cingulate input to the primary and supplementary motor cortices in the rhesus monkey: evidence for somatotopy in areas 24c and 23c. J. Comp. Neurol 322, 471–489. doi: 10.1002/cne.903220403. [PubMed: 1383283]

Ohayon S, Grimaldi P, Schweers N, Tsao DY, 2013. Saccade modulation by optical and electrical stimulation in the macaque frontal eye field. J. Neurosci 33, 16684–16697. doi: 10.1523/JNEUROSCI.2675-13.2013. [PubMed: 24133271]

Pitkänen A, Amaral DG, 1991. Demonstration of projections from the lateral nucleus to the basal nucleus of the amygdala: a PHA-L study in the monkey. Exp. Brain Res 83, 465–470. [PubMed: 1709111]

Price JL, 1999. Prefrontal cortical networks related to visceral function and mood. In: Annals of the New York Academy of Sciences. New York Academy of Sciences, pp. 383–396. doi: 10.1111/j.1749-6632.1999.tb09278.x.

Reveley C, Gruslys A, Ye FQ, Glen D, Samaha J, E Russ B, Saad Z, K Seth A, Leopold DA, Saleem KS, 2017. Three-dimensional digital template Atlas of the Macaque brain. Cereb. Cortex N. Y. N 1991 27, 4463–4477. doi: 10.1093/cer-cor/bhw248.

Saleem KS, Logothetis NK, 2012. A Combined MRI and Histology Atlas of the Rhesus Monkey Brain in Stereotaxic Coordinates. Elsevier, Academic Press.

Shapiro MG, Homma K, Villarreal S, Richter C−P, Bezanilla F, 2012. Infrared light excites cells by changing their electrical capacitance. Nat. Commun 3, 736. doi: 10.1038/ncomms1742. [PubMed: 22415827]

Sharma KK, Kelly EA, Pfeifer CW, Fudge JL, 2020. Translating fear circuitry: amygdala projections to subgenual and perigenual anterior cingulate in the Macaque. Cereb. Cortex N. Y. N 1991 30, 550–562. doi: 10.1093/cercor/bhz106.

Smiley JF, Hackett TA, Ulbert I, Karmas G, Lakatos P, Javitt DC, Schroeder CE, 2007. Multisensory convergence in auditory cortex, I. Cortical connections of the caudal superior temporal plane in macaque monkeys. J. Comp. Neurol 502, 894–923. doi: 10.1002/cne.21325. [PubMed: 17447261]

Stefanacci L, Amaral DG, 2002. Some observations on cortical inputs to the macaque monkey amygdala: an anterograde tracing study. J. Comp. Neurol 451, 301–323. doi: 10.1002/cne.10339. [PubMed: 12210126]

Tan X, Jahan I, Xu Y, Stock S, Kwan CC, Soriano C, Xiao X, García-Añoveros J, Fritzsch B, Richter C−.P., 2018. Auditory neural activity in congenitally deaf mice induced by infrared neural stimulation. Sci. Rep 8, 388. doi: 10.1038/s41598-017-18814-9. [PubMed: 29321651]

Tomasi D, Volkow ND, 2011. Association between functional connectivity hubs and brain networks. Cereb. Cortex 21. doi: 10.1093/cercor/bhq268, 2003–2013.

Wells J, Kao C, Jansen ED, Konrad P, Mahadevan-Jansen A, 2005a. Application of infrared light for in vivo neural stimulation. J. Biomed. Opt 10, 064003. doi: 10.1117/1.2121772.

Wells J, Kao C, Mariappan K, Albea J, Jansen ED, Konrad P, Mahadevan–Jansen A, 2005b. Optical stimulation of neural tissue in vivo. Opt. Lett 30, 504–506. [PubMed: 15789717]

Xu AG, Qian M, Tian F, Xu B, Friedman RM, Wang J, Song X, Sun Y, Chernov MM, Cayce JM, Jansen ED, Mahadevan-Jansen A, Zhang X, Chen G, Roe AW, 2019. Focal infrared neural stimulation with high-field functional MRI: a rapid way to map mesoscale brain connectomes. Sci. Adv 5. doi: 10.1126/sci-adv.aau7046.

Yukie M, 2002. Connections between the amygdala and auditory cortical areas in the macaque monkey. Neurosci. Res 42, 219–229. doi: 10.1016/s0168-0102(01)00325-x. [PubMed: 11900831]

Zhang X, Xu AG, Xi W, Roe AW, 2019. Quantifying Tissue Temperature Change Induced by Infrared Neural Stimulation by 7T MR Thermometry. SPIE Photonics West, San Francisco, CA.

Zhu X, Lin J−.W., Sander, M.Y., 2019. Infrared inhibition and waveform modulation of action potentials in the crayfish motor axon. Biomed. Opt. Express 10, 6580–6594. doi: 10.1364/BOE.10.006580. [PubMed: 31853418]

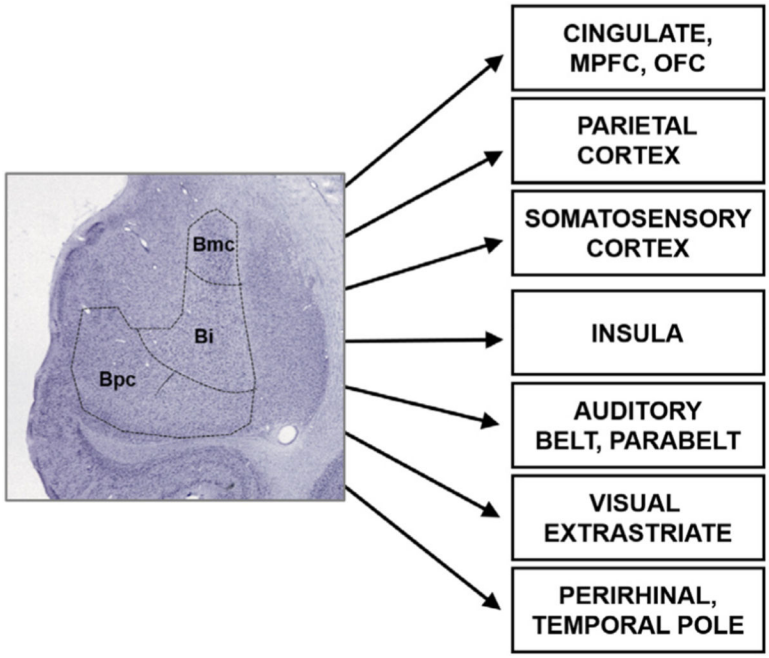

Fig. 1.

Connections of the basal nucleus of the amygdala in the macaque monkey. References are listed in Supplementary information Appendix A.

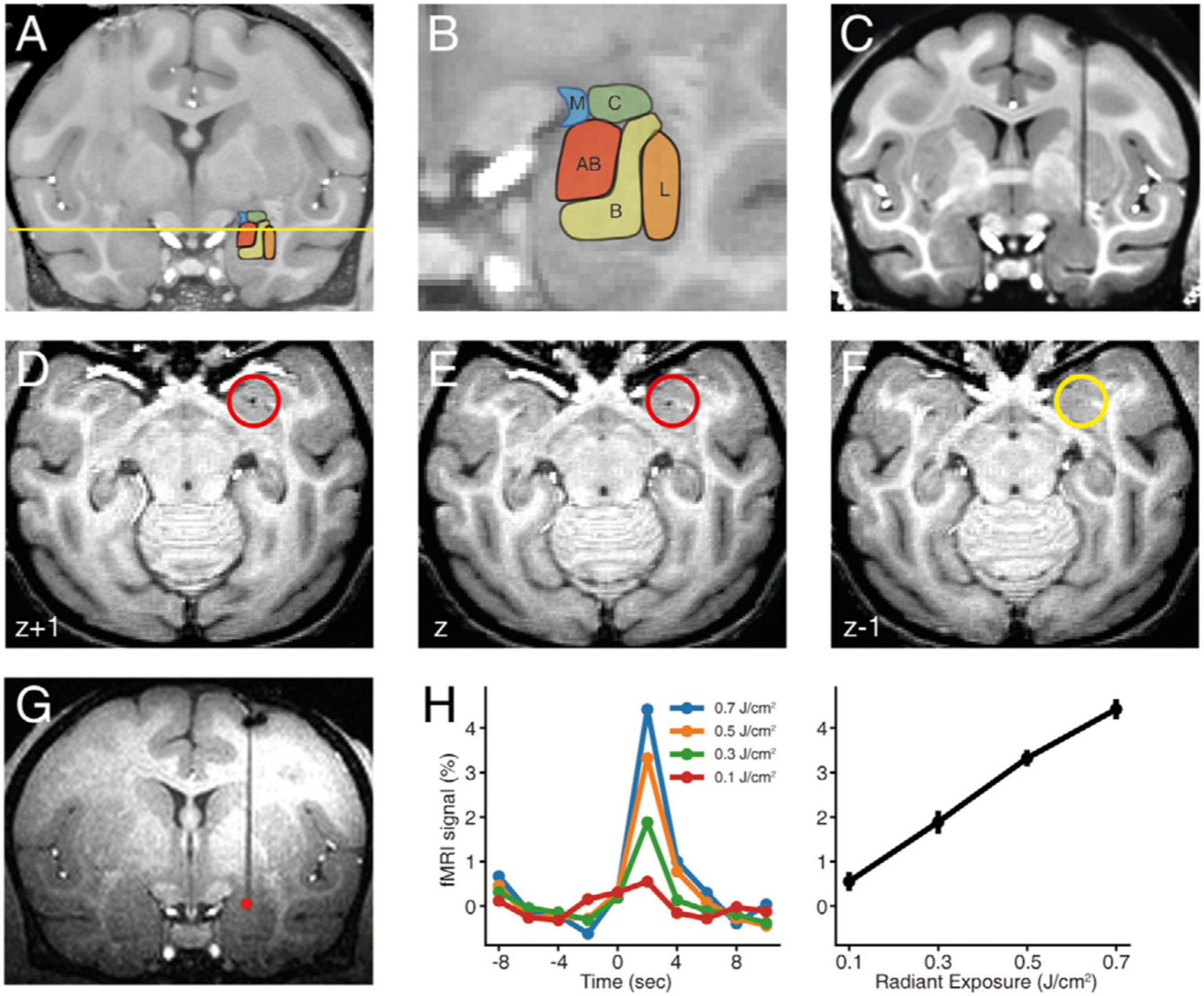

Fig. 2. Anatomical localization and intensity-dependence of INS stimulation.

A-B. Amygdala nuclei in macaque monkey. Labels: L, B, AB, C, and M stand for the lateral, basal, accessory basal, central and medial nuclei of the amygdala respectively. **C-F.** *Localization of fiber tip*. C: determination of fiber position shown in coronal plane. d -F: The depth of fiber tip was localized in the ventralmost horizontal section (E) with visible signal dropout due to the laser tip (red circle: location of tip) (signal dropout is absent in F). In this example, the tip is in the magnocellular subdivision of the basal nucleus of the amygdala (depth indicated by yellow line in A). **G**. Activation at the laser tip, 0.3 J/cm^2. **H**. *Intensity dependence.* Left: Time courses of the fMRI signals at the laser tip. As previously described (Xu et al., 2019), at the laser tip, peaks occur at a latency of ~2 s from stimulation onset. Right: Relationship between laser intensity and peak response amplitude at fiber tip. Error bars: SEM. (For interpretation of the references to color in this figure legend, the reader is referred to the web version of this article.)

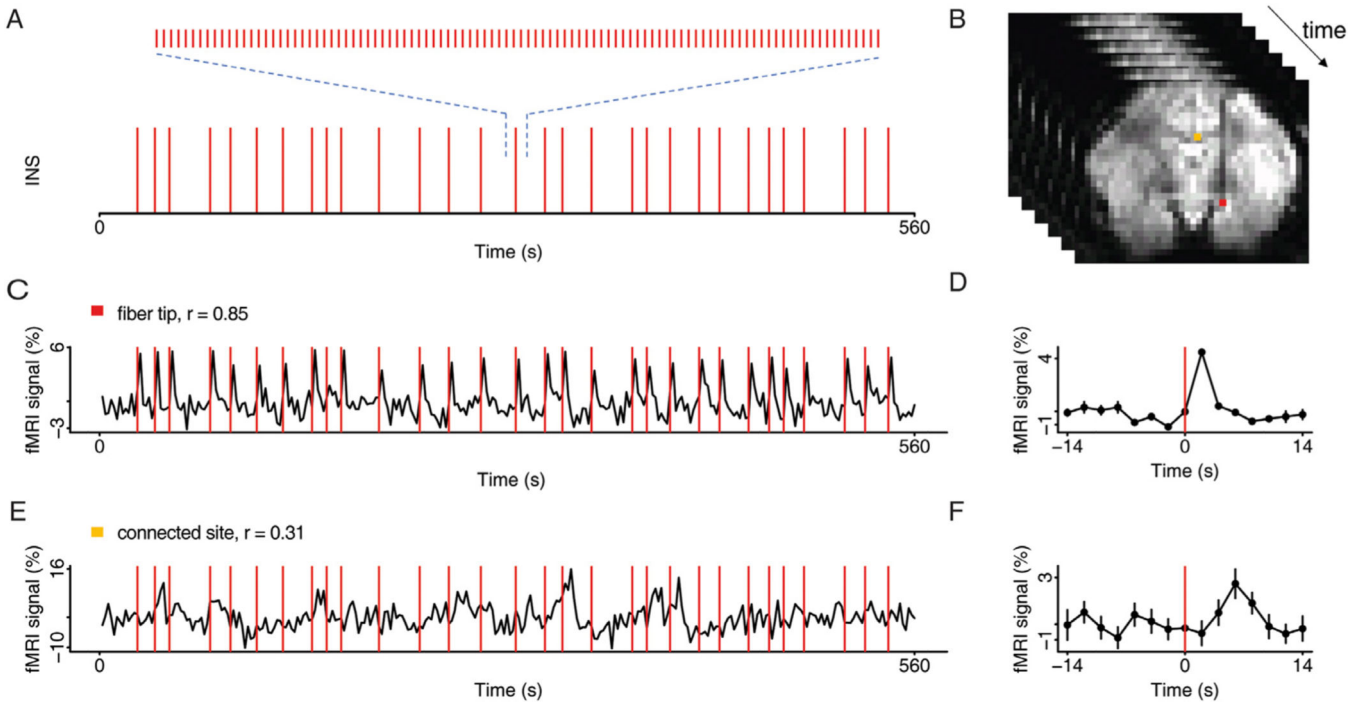

Fig. 3. INS stimulation paradigm.

A. Temporal distribution of INS pulse trains triggered at random onsets. Each pulse train (0.5 s, 200hz, 250us/pulse) consists of 100 laser pulses (shown expanded above). **B**. Example of functional images acquired over time, with highlights of the activated voxels at the stimulation site (red voxel) and at the presumed connected site (orange voxel) ($p < 0.001$). **C**. Time course of the fMRI signals at the laser tip in response to stimulation in A (red voxel in B). Stimulation timepoints (red lines) superimposed on BOLD trace. Correlation values (r) indicated above each trace. **D**. Time course averaged over repetitions (in C). **E**. Time course of the fMRI signals at a presumed connected site in response to stimulation in A (orange voxel in B). **F**. Time course averaged over repetitions (in E). Error bars: SEM. Stimulation intensity 0.5 J/cm^2. (For interpretation of the references to color in this figure legend, the reader is referred to the web version of this article.)

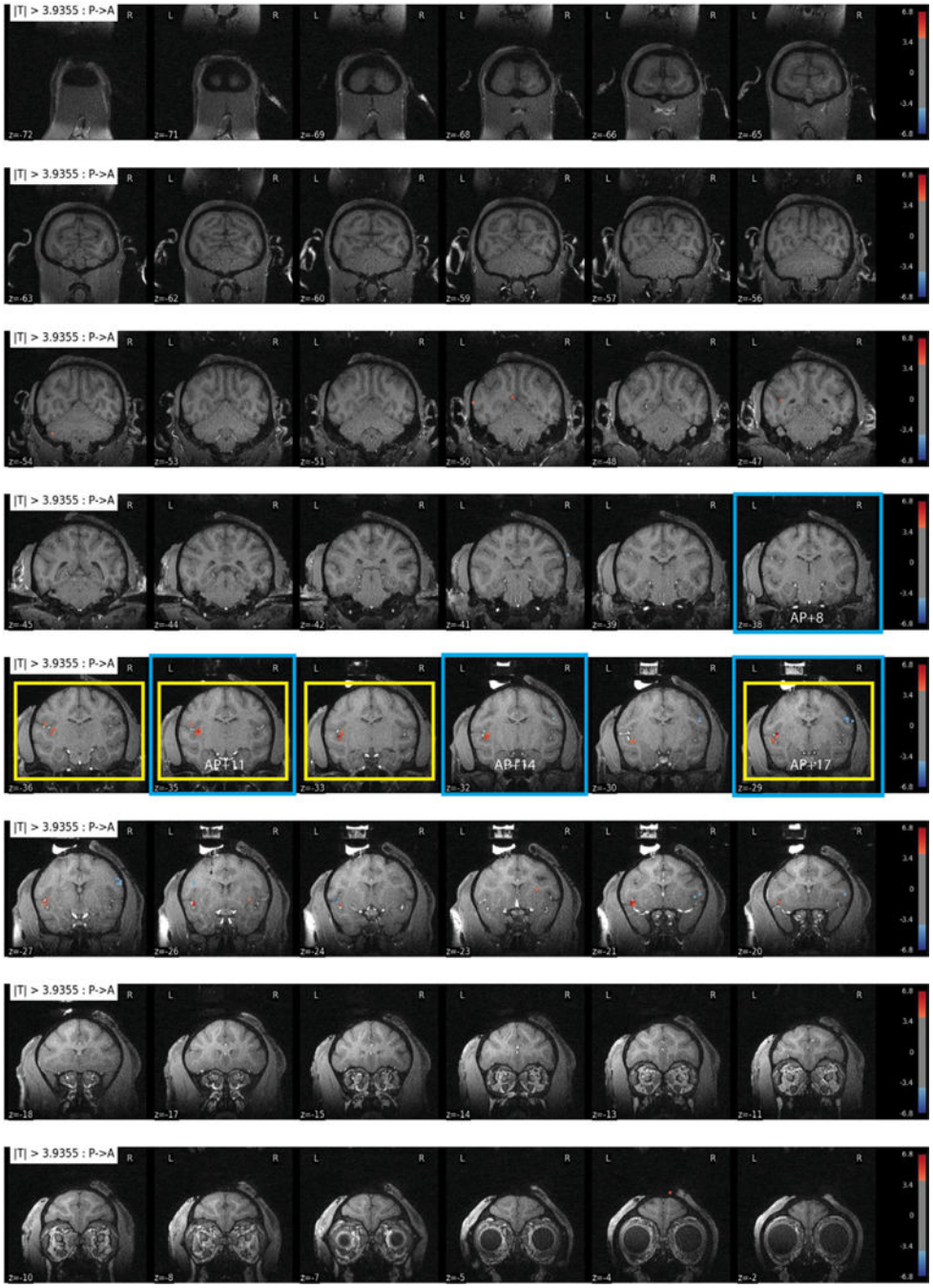

Fig. 4.

All slices from a stimulation site in basal nucleus of the amygdala in Monkey M. Site 28 stimulation (0.1 J/cm^2, $p < 0.0001$, FDR 5.5%); this site contributed to Fig. 5E–H and Fig. 7D (slices outlined in yellow and blue, respectively). (For interpretation of the references to color in this figure legend, the reader is referred to the web version of this article.)

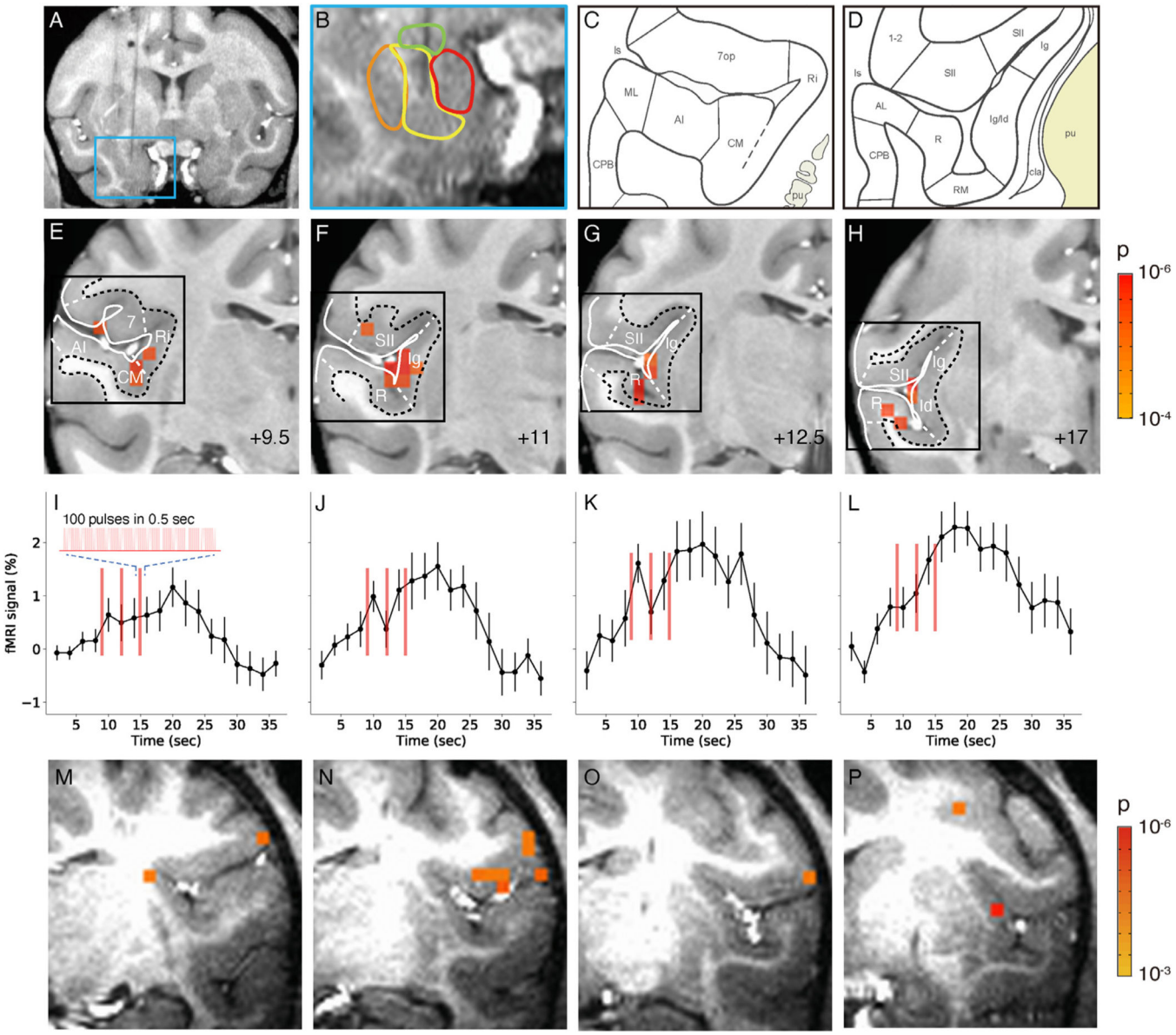

Fig. 5. Activation in insula and lateral sulcal areas elicited by stimulation of the basal nucleus of the amygdala.

A-L. Monkey M. M-P. Monkey Y. A-B. Stimulation site in intermediate zone of the basal nucleus. C-D. Schematics of cortical areas in the lateral sulcus, including insular cortical areas. insula: lg, ld, Ri. Auditory areas: AI, CM, ML, R, RM. Somatosensory areas: SII, 1–2. (Saleem and Logothetis, 2012) E-H. Activations within the lateral sulcus from posterior (+9.5) to anterior (+17) (9.5 mm, 11 mm, 12,5 mm,17 mm, respectively). Voxels: $p < 0.0001$ (FDR 5.5%). Black box: approximate regions shown in C-D. I-L: Associated time courses of fMRI signal in E-H (mean of significant voxels). Inset: enlarged schematic of each stimulus train (red line). Stimulation: block design, 0.1 J/cm^2. Error bars: SEM. M-P. Activations within the lateral sulcus are seen in monkey Y. Voxels: $p < 0.001$.

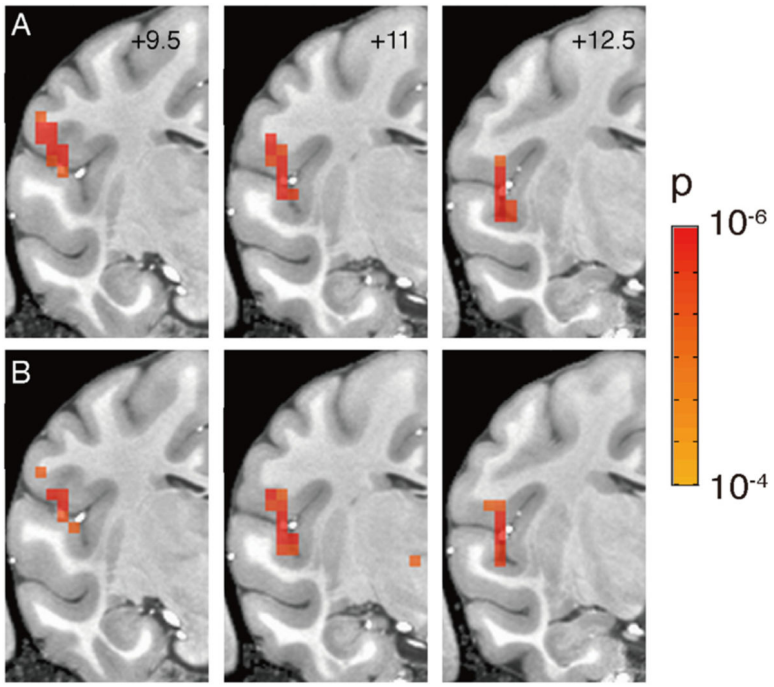

Fig. 6. Reliability of activation patterns.

Half-trial (total $n = 20$) comparisons of activation following focal stimulation from a single site in the basal nucleus of amygdala (site E in Fig. 7, block design, 0.1 J/cm^2). **A-B.** Three consecutive sections (AP: +9.5, +11, +12.5) showing activation maps obtained from 10 odd (**A**) and 10 even (**B**) trials. ($p < 0.0001$, FDR 6.7%).

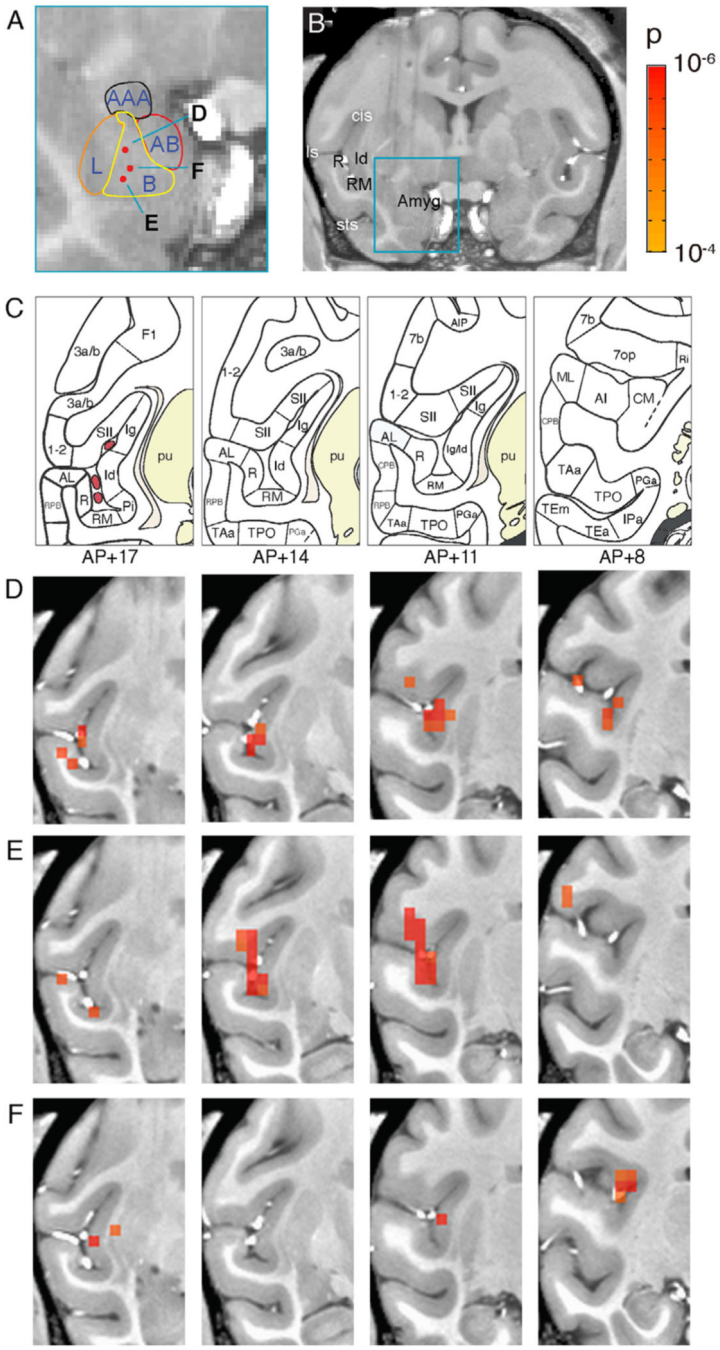

Fig. 7. Topography of cortical connectivity with basal nucleus of amygdala.

A-B. Estimated nuclear boundaries in the amygdala and the anatomical location of three stimulation sites shown as red dots and marked as D, E, and F. **C.** Parcellation of the insula and the surrounding temporal sulcal areas based on the Saleem and Logothetis atlas. **D-F**. Series of coronal activation maps corresponding to the stimulation sites D, E, and F in the basal nucleus (panel A). The maps are arranged from left to right in an anterior-to-posterior progression (AP: +17, +14, +11, +8). Voxels thresholded at $p < 0.0001$ (FDR D: 5.5%, E: 14%, F: 6.7%). Stimulation: block design, 0.1 J/cm^2.

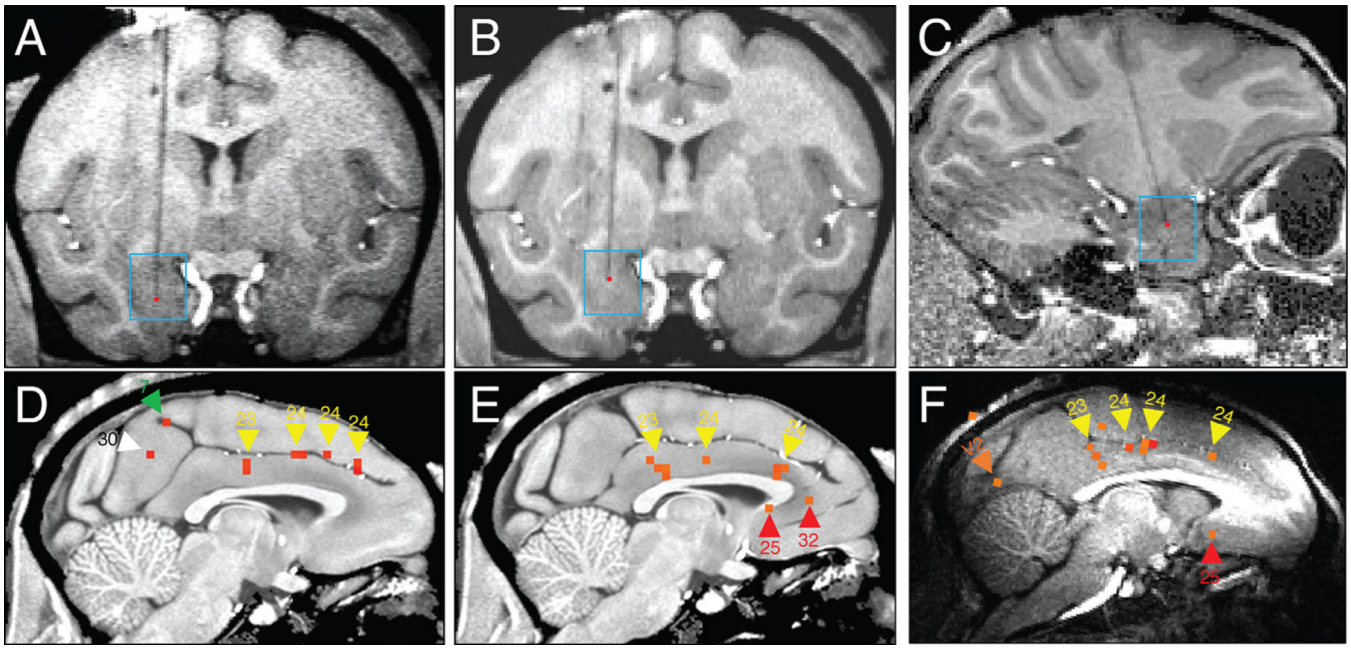

Fig. 8. Focal and patchy nature of remote responses.

Stimulation of basal nucleus in amygdala induces responses in the ipsilateral cingulate cortex. 3 examples shown. **A-C**. Stimulation sites (red dots) of **D,E,F**, respectively. **D-F:** Activations in cingulate. **D:** Monkey M site #46 (GLM $p < 0.0001$, FDR 11.6%), **E:** Monkey M site #27 (permutation $p < 0.002$; also see Supp Fig. 1). **F:** Monkey Y (GLM $p < 0.001$). Activations indicated by arrowheads: *Yellow* (cingulate 23, 24), *White* (retrosplenial 29/30), *Red* (medial prefrontal 25, 32), *Orange* (visual V2). Monkey M block design, 0.1 J/cm^2. Monkey Y event-related design, 0.1 J/cm^2.